Sound & Vibration 2026, 60(3), 4070.
doi: https://doi.org/10.59400/sv4070

Article

Fuzzy-stochastic coupled models for broadband noise radiation from flexible

Suleiman Ibrahim Mohammad[1], Yogeesh Nijalingappa[1,2,*], Basem Abu Zneid[3], Shashikumar Honnavalli Channabasavaiah[4], Asokan Vasudevan[5], Jayaprakasha Pathiyappanapallya Chandraiah[6]

[1] Research Fellow, INTI International University, Nilai 71800, Malaysia
[2] Department of Mathematics, Government First Grade College, Tumkur 572102, India
[3] Faculty of Engineering, Hourani Center for Applied Scientific Research, Al-Ahliyya Amman University, Amman 19111, Jordan
[4] Department of Mathematics, Government First Grade College, Tiptur 572201, India
[5] Faculty of Business and Communications, INTI International University, Nilai 71800, Malaysia
[6] Department of Mathematics, Government First Grade College for Women, Tumkur 572102, India
*** Corresponding author:** Yogeesh Nijalingappa, yogeesh.r@gmail.com

CITATION

Mohammad SI, Nijalingappa Y, Zneid BA, et al. Fuzzy-stochastic coupled models for broadband noise radiation from flexible. Sound & Vibration. 2026; 60(3): 4070. https://doi.org/10.59400/sv4070

ARTICLE INFO

Received: 25 February 2026
Revised: 15 March 2026
Accepted: 20 March 2026
Available online: 30 April 2026

Abstract: Broadband noise radiation from flexible panels is governed by the coupling of random excitation fields with uncertain structural and boundary parameters. This paper develops a fuzzy-stochastic vibro-acoustic framework that separates (i) aleatory uncertainty in the broadband pressure field from (ii) epistemic uncertainty in panel properties and mount conditions. The panel dynamics are modeled in the frequency domain using a modal or finite-element representation of the thin-plate operator, while acoustic radiation is evaluated through a baffle-mounted radiation model leading to radiated sound power spectra. Random excitation is represented by the pressure cross spectral density, enabling direct propagation of spectral statistics to displacement and velocity cross-spectra via linear transfer functions. Epistemic uncertainty in Young's modulus, thickness, and loss factor is represented by fuzzy numbers and propagated through α-cuts, yielding interval-valued parameter sets at each α level. The coupling is implemented using an α-cut outer loop with a stochastic inner solver that computes mean and variance of radiated sound power; α-level interval extrema then provide fuzzy envelopes of stochastic response metrics. Verification is performed through modal truncation, frequency-grid stability, and α-grid refinement. Numerical demonstrations using representative datasets show that epistemic uncertainty can induce wide bands in band-integrated sound power level (≈9.9 dB in the 100–1,000 Hz band at $\alpha = 0$), and that percentile metrics (e.g., 95th percentile under a lognormal approximation) provide conservative bounds for design decision-making. The proposed framework offers a transparent and computationally tractable route to uncertainty-aware broadband vibro-acoustic prediction for panels in vehicles, buildings, and machinery enclosures.

Keywords: broadband vibro-acoustics; flexible panels; radiated sound power; fuzzy sets; α-cuts; random vibration; cross-spectral density; uncertainty quantification

1. Introduction and contributions

Broadband noise radiation from flexible panels is a central problem in vibro-acoustics because panels act as efficient transducers from distributed pressure excitation (aerodynamic turbulence, machinery broadband forcing, road-induced vibro-loads, etc.) to airborne sound [1, 2]. In practical settings, uncertainty enters in two fundamentally different ways: Recent reliability and uncertainty-quantification

studies also support this separation of aleatory and epistemic components and motivate surrogate-assisted propagation when direct analysis is expensive [3].

Recent vibro-acoustic and acoustic-uncertainty studies on diffuse sound insulation, half-space scattering, and coupled plate-cavity systems further show that uncertainty treatment is increasingly important in practical acoustic prediction and design.

Aleatory uncertainty (randomness): the excitation is intrinsically random (a random field) and is best described through power spectral density (PSD) and cross-spectral density (CSD) functions [3,4].

Epistemic uncertainty (imprecision): material properties, damping, mounting stiffness, boundary conditions, and manufacturing tolerances are not precisely known; these are naturally represented by fuzzy sets when data are scarce or expert ranges are used [5,6].

Most existing broadband vibro-acoustic models treat uncertainty as purely stochastic (probability distributions for all parameters) or purely fuzzy. However, broadband acoustic radiation often requires both randomness (excitation) and imprecision (parameters), motivating a fuzzy-stochastic coupled model.

1.1. Problem statement

Given a flexible panel occupying surface $S \subset \mathrm{R}^2$ (**Figure 1**), excited by a broadband pressure field $p(\mathrm{x}, t)$, the objectives are to:

- Predict radiated sound power spectrum $W(\omega)$ (or SPL/Lw metrics);
- Quantify uncertainty via fuzzy bounds (α-cut envelopes) on stochastic summaries such as, percentiles, and band-integrated levels.

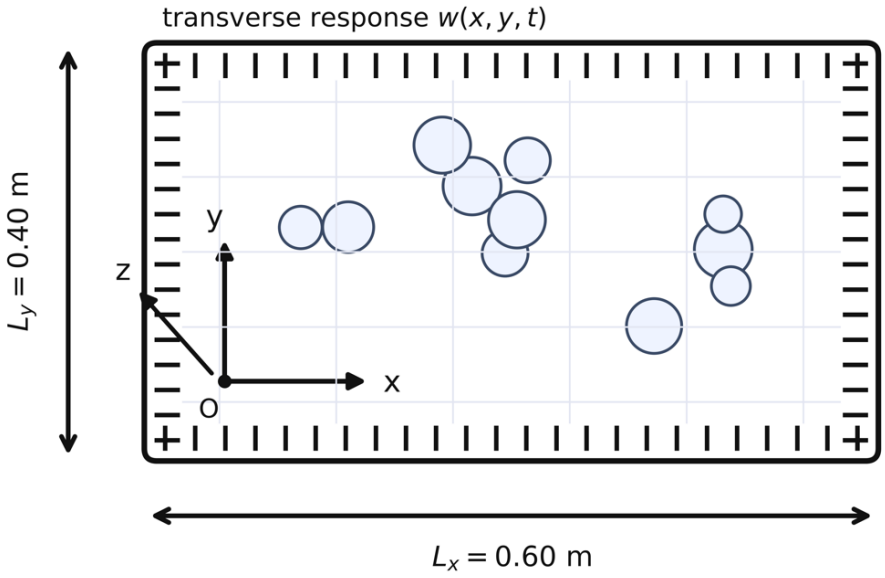

Figure 1. Flexible panel geometry, coordinates, and clamped boundaries.

1.2. Contributions

This paper develops a coupled uncertainty framework in which:

- The excitation is modeled as a wide-sense stationary stochastic field using PSD/CSD descriptions [3,4];

- Key structural and boundary parameters are represented as fuzzy numbers and propagated using α-cuts;
- The resulting output is a fuzzy family of stochastic responses, producing α-level intervals of spectral and broadband acoustic metrics.

The excitation randomness is carried by PSD/CSD functions, while uncertain panel parameters are represented fuzzily. The model maps Φ_{pp} and $\widetilde{\Theta}$ into fuzzy envelopes of $W(\omega)$ and broadband levels.

2. Deterministic vibro-acoustic model (baseline mapping $\Theta \mapsto W(\omega)$)

This section defines the deterministic forward model that will later be embedded in the stochastic and fuzzy layers.

2.1. Panel dynamics in the frequency domain

Consider a thin isotropic Kirchhoff-Love plate of thickness h, density ϱ_s, Young's modulus E, and Poisson's ratio v. Let $w(\mathrm{x}, t)$ denote transverse displacement, $\mathrm{x} = (x, y) \in S$. In the frequency domain (Fourier transform convention $e^{i\omega t}$), the governing equation is [1, 2]:

$$D\nabla^4 w(\mathbf{x}, \omega) - \varrho_s h\omega^2 w(\mathbf{x}, \omega) + i\omega c_d w(\mathbf{x}, \omega) = p(\mathbf{x}, \omega), \tag{1}$$

where

$$D = \frac{Eh^3}{12\,(1 - v^2)} \tag{2}$$

is the bending stiffness and c_d is an equivalent viscous damping coefficient (or can be defined via modal loss factor η; see below).

Explanation:

- The operator $D\nabla^4$ captures bending resistance.
- The term $\varrho_s h\omega^2$ is the inertial contribution.
- The term $i\omega c_d$ represents dissipation; for structural loss factor η, one commonly uses a complex stiffness $D(1 + i\eta)$ instead of c_d [1,2].

2.2. Modal formulation (computationally efficient for broadband)

Let $\{\phi_r(\mathbf{x})\}_{r=1}^{N_m}$ be mode shapes satisfying the boundary conditions (clamped, simply supported, elastic restraint, etc.). Expand:

$$w(\mathbf{x}, \omega) = \sum\nolimits_{r=1}^{N_m} \phi_r(\mathbf{x}) q_r(\omega). \tag{3}$$

Projecting (1) onto ϕ_r yields the modal transfer function:

$$q_r(\omega) = \frac{f_r(\omega)}{k_r - \omega^2 m_r + i\omega c_r},\ f_r(\omega) = \int_S \phi_r(\mathbf{x}) p(\mathbf{x}, \omega) dS, \tag{4}$$

where m_r, k_r, c_r are generalized modal mass, stiffness, and damping, respectively. If

damping is represented by loss factor η_r, then:

$$k_r \to k_r\left(1+i\eta_r\right),\ \text{so}\ q_r(\omega)=\frac{f_r(\omega)}{k_r\left(1+i\eta_r\right)-\omega^2 m_r}. \tag{5}$$

Why modal form matters for this study.

In broadband problems, the output metrics require integrating across frequency bands. Modal forms allow rapid evaluation across a dense frequency grid and naturally connect to spectral (PSD/CSD) propagation in Section 3 [2,4].

2.3. Acoustic radiation from panel velocity (Rayleigh integral)

Let the panel be mounted in an infinite rigid baffle (a standard first model for radiation efficiency studies) so that the radiated pressure at a field point **r** is [1, 2]:

$$p_a(\mathbf{r},\omega)=i\varrho_0 c_0 k\int_S \frac{v(\mathbf{x},\omega)e^{-ikR}}{2\pi R}dS,\ v(\mathbf{x},\omega)=i\omega w(\mathbf{x},\omega), \tag{6}$$

where $k=\omega/c_0, R=\|\mathbf{r}-\mathbf{x}\|,\ \varrho_0$ is air density, and c_0 is speed of sound.

The time-averaged radiated sound power is:

$$W(\omega)=\frac{1}{2}\Re\left\{\int_S p_a(\mathbf{x},\omega)v^*(\mathbf{x},\omega)dS\right\}. \tag{7}$$

For engineering interpretation, define radiation efficiency $\sigma(\omega)$ [1,2]:

$$W(\omega)=\ \varrho_0 c_0 S\sigma(\omega)\left\langle|v(\mathbf{x},\omega)|^2\right\rangle_S, \tag{8}$$

where $\langle\cdot\rangle_S$ denotes spatial averaging over S.

Deterministic forward map:

Equations (1)–(8) define the deterministic mapping:

$$(\Theta,p(\cdot,\omega))\longmapsto w(\cdot,\omega)\longmapsto v(\cdot,\omega)\longmapsto W(\omega), \tag{9}$$

with parameter vector

$$\Theta=\{E,v,\varrho_s,h,\eta\,(\text{or}\ c_d),\ \text{boundary parameters}\}. \tag{10}$$

Rectangular panel $0\le x\le L_x, 0\le y\le L_y$ with representative clamped constraints (ticks). The formulation supports alternative boundary models (simply supported or elastic restraints) through the modal basis or FE matrices.

The below **Table 1** shows the acoustic parameters and their representative symbols which are used in this study.

Table 1. Representative panel and acoustic parameters.

Symbol	Meaning	Baseline value	Units	Uncertainty type (later sections)
L	panel length	0.60	m	crisp
W	panel width	0.40	m	crisp
h	thickness	1.5×10^{-3}	m	fuzzy (manufacturing)

Table 1. *Cont.*

ρ_s	panel density	2,700	kg/m^3	fuzzy (batch variability)
E	Young's modulus	70×10^9	Pa	fuzzy (effective modulus)
ν	Poisson ratio	0.33	-	crisp/fuzzy (minor)
η	loss factor	0.02	-	fuzzy (assembly dependent)
ρ_0	air density	1.20	kg/m³	crisp
c_0	speed of sound	343	m/s	crisp

Note: Use this parameter set to generate numerical curves and verify scaling; values are typical engineering data for aluminum panels and air at room conditions [1,2].

3. Stochastic excitation model and broadband acoustic metrics

In real environments, pressure excitation is not deterministic. A mathematically consistent broadband model treats $p(\mathbf{x}, t)$ as a zero-mean wide-sense stationary random field [3,4].

3.1. PSD and CSD of the pressure field

Let $P(\mathbf{x}, \omega)$ be the Fourier transform of $p(\mathbf{x}, t)$. Define the cross-spectral density:

$$\Phi_{pp}\left(\mathbf{x}_1, \mathbf{x}_2; \omega\right) = \mathrm{E}\left[P\left(\mathbf{x}_1, \omega\right) P^*\left(\mathbf{x}_2, \omega\right)\right], \tag{11}$$

and the point PSD as the diagonal:

$$S_{pp}(\mathbf{x}; \omega) = \Phi_{pp}(\mathbf{x}, \mathbf{x}; \omega). \tag{12}$$

A common separable model used in panel excitation studies is:

$$\Phi_{pp}\left(\mathbf{x}_1, \mathbf{x}_2; \omega\right) = \sqrt{S_{pp}\left(\mathbf{x}_1; \omega\right) S_{pp}\left(\mathbf{x}_2; \omega\right)}\, \gamma_{pp}\left(\left\|\mathbf{x}_1 - \mathbf{x}_2\right\|, \omega\right), \tag{13}$$

where γ_{pp} is a coherence function satisfying $|\gamma_{pp}| \leq 1$ and $\gamma_{pp}(0, \omega) = 1$ [3,4].

Excitation used for numerical demonstrations:

For a practical broadband spectrum (**Figure 2**), adopt a smooth PSD shape:

$$S_{pp}(\omega) = S_0 \frac{1}{1 + (\omega/\omega_1)^2} \frac{1}{1 + (\omega_2/\omega)^6} \tag{14}$$

which produces a band-limited broadband forcing (low/high roll-offs). Spatial coherence can be modeled as:

$$\gamma_{pp}(r, \omega) = \exp\left(-r/L_c\right) \exp(-\beta\omega), \tag{15}$$

where L_c is a coherence length and β controls the decay with frequency (**Figure 3**). This form is consistent with widely used coherence modeling in random vibration/signal processing (physically: pressure becomes less coherent at higher frequencies and larger separations) [3,4].

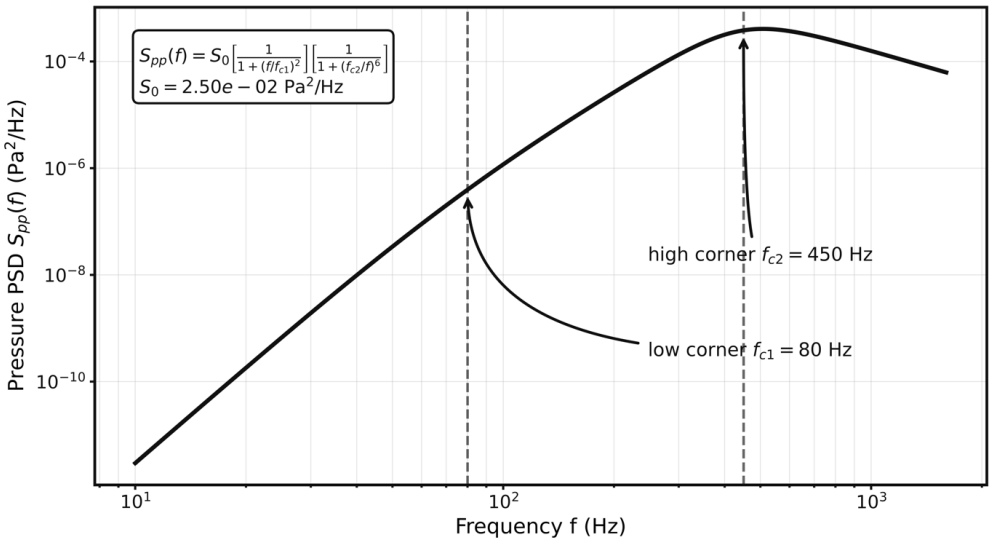

Figure 2. Example broadband excitation: Pressure PSD.

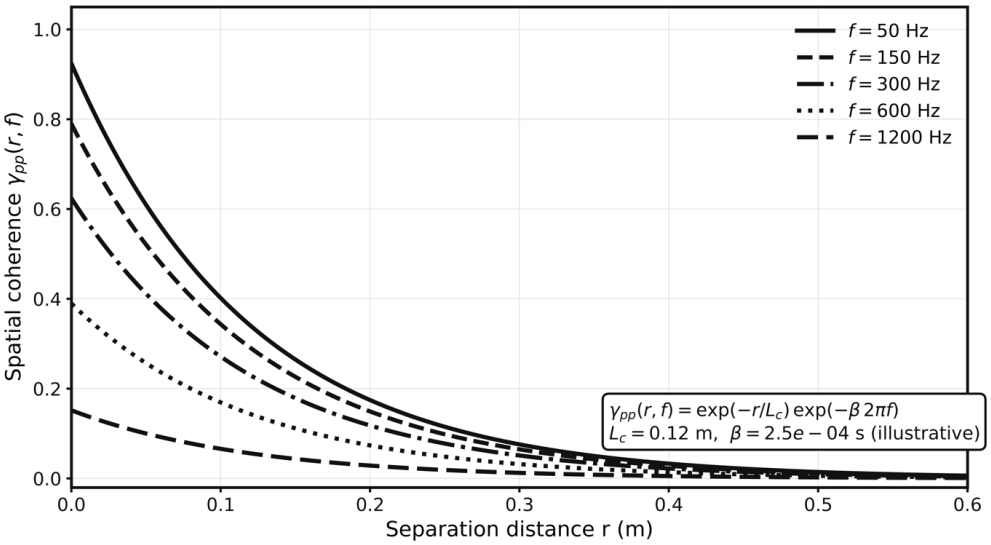

Figure 3. Spatial coherence decay with frequency and separation (example).

A representative broadband pressure PSD $S_{pp}(f)$ used to demonstrate the framework. The specific parametric form is given by Equation (14) and is selected to mimic typical bandlimited broadband excitations encountered in vibro-acoustic practice.

Coherence magnitude $|\gamma_{pp}(r, f)|$ for several separations r, illustrating decreasing spatial correlation at higher frequency and larger distance, consistent with the model in Equation (15).

3.2. Propagation of excitation spectra to structural response spectra

Because the panel dynamics are linear (Section 2), spectral propagation is systematic. Let the displacement be expressed by modal coordinates (3)–(5). Define the modal force:

$$F_r(\omega) = \int_S \phi_r(\mathbf{x}) P(\mathbf{x}, \omega) dS. \tag{16}$$

Then:

$$Q_r(\omega) = H_r(\omega)F_r(\omega),\ H_r(\omega) = \frac{1}{k_r - \omega^2 m_r + i\omega c_r}. \tag{17}$$

The modal CSD becomes:

$$\Phi_{Q_rQ_s}(\omega) = H_r(\omega)H_s^*(\omega)\Phi_{F_rF_s}(\omega), \tag{18}$$

with

$$\Phi_{F_rF_s}(\omega) = E\left[F_r(\omega)F_s^*(\omega)\right] = \int_S \int_S \phi_r\left(\mathbf{x}_1\right)\phi_s\left(\mathbf{x}_2\right)\Phi_{pp}\left(\mathbf{x}_1, \mathbf{x}_2; \omega\right) dS_1 dS_2. \tag{19}$$

Finally, the displacement CSD at two panel points is:

$$\Phi_{ww}\left(\mathbf{x}_a, \mathbf{x}_b; \omega\right) = \sum\nolimits_{r=1}^{N_m} \sum\nolimits_{s=1}^{N_m} \phi_r\left(\mathbf{x}_a\right)\phi_s\left(\mathbf{x}_b\right)\Phi_{Q_rQ_s}(\omega). \tag{20}$$

Velocity spectra follow from $v = i\omega w$:

$$\Phi_{vv}\left(\mathbf{x}_a, \mathbf{x}_b; \omega\right) = \omega^2 \Phi_{ww}\left(\mathbf{x}_a, \mathbf{x}_b; \omega\right). \tag{21}$$

Interpretation:

Equation (19) is the key bridge: it shows how the pressure-field CSD injects randomness into the modal forces, which then propagate through the modal transfer functions to produce response CSDs. This is standard random vibration/spectral analysis, and it is the exact place where later fuzzy parameter uncertainty will couple into the stochastic response. For numerical discretization, Equation (19) is evaluated by element-wise surface quadrature after interpolating the pressure CSD and mode shapes on the same mesh; for irregular boundaries or non-analytical modes, standard FE shape functions and Gaussian quadrature are used, so the projection kernel remains regular and no additional singular treatment is required in this step.

3.3. Stochastic broadband acoustic metrics

The acoustic metric of interest is often the expected radiated sound power spectrum:

$$\mu_W(\omega) = \mathrm{E}[W(\omega)], \tag{22}$$

and possibly a variance (or confidence band) of $W(\omega)$:

$$\sigma_W^2(\omega) = \mathrm{Var}[W(\omega)]. \tag{23}$$

For practical reporting, one uses band-integrated power over $[\omega_1, \omega_2]$:

$$W_{\text{band}} = \int_{\omega_1}^{\omega_2} W(\omega)d\omega,\ \mu_{W,\text{ band}} = \int_{\omega_1}^{\omega_2} \mu_W(\omega)d\omega \tag{24}$$

and sound power level:

$$L_W(\omega) = 10\log_{10}\left(\frac{W(\omega)}{W_{\text{ref}}}\right),\ W_{\text{ref}} = 10^{-12}\text{W}. \tag{25}$$

The Stochastic excitation model which are used in this study are represented in the **Table 2** below.

Table 2. Stochastic excitation model used in this study (for Sections 3 and later numerical results).

Component	Mathematical object	Model used here	Notes
Pressure PSD	$S_{pp}(x, x', f)$	Equation (14)	Band-limited broadband spectrum (**Figure 2**)
Spatial coherence	$\gamma(\lvert x - x'\rvert, f)$	Equation (15)	Decays with separation and frequency (**Figure 3**)
Pressure CSD	S_{pp}	Equation (13)	Builds full random-field description
Modal force CSD	$S_{QmQn}(f)$	Equation (19)	Double integral projection onto modes
Response CSD	$S_{ww}(x, x', f)$	Equations (20) and (21)	Enables spectral output metrics

4. Fuzzy modelling of epistemic uncertainty in panel parameters and boundary conditions

Broadband panel radiation predictions require parameters that are rarely known precisely in real installations (assembly-dependent damping, thickness tolerance, effective stiffness under fastening, etc.). When information is available mainly as ranges (manufacturer tolerance bands, expert judgment, sparse measurements), a fuzzy set representation is appropriate for epistemic uncertainty [7, 8]. In this work, key components of the deterministic parameter vector Θ (Equation (10)) are modeled as fuzzy numbers:

$$\widetilde{\Theta} = \left\{\widetilde{E}, \widetilde{h}, \widetilde{\eta}, \widetilde{\varrho}_s, \widetilde{k}_b, \ldots\right\}, \tag{26}$$

where $\widetilde{k}_b$ can represent uncertain boundary restraint (e.g., elastic edge stiffness).

4.1. Fuzzy numbers and membership functions

A fuzzy number $\widetilde{x}$ on R is defined by a membership function $\mu_{\widetilde{x}} : R \to [0, 1]$. For engineering parameters, triangular and trapezoidal fuzzy numbers are common due to interpretability and the ability to encode "most likely" and "plausible extremes" [8].

Triangular fuzzy number (TFN):

A TFN $\widetilde{x} = \left(x^L, x^M, x^U\right)$ has membership

$$\mu_{\widetilde{x}}(x) = \begin{cases} 0, & x < x^L \\ \frac{x - x^L}{x^M - x^L}, & x^L \le x \le x^M \\ \frac{x^U - x}{x^U - x^M}, & x^M \le x \le x^U \\ 0, & x > x^U \end{cases} \tag{27}$$

Engineering meaning:

- x^L: conservative minimum plausible value;
- x^M: nominal/most plausible value;

- x^U: conservative maximum plausible value.

In this paper's baseline dataset (**Table 3**), we use TFNs for, and, reflecting typical manufacturing and assembly variability for thin metal panels and loss-factor uncertainty [8]. The asymmetric loss-factor TFN in **Table 3** is therefore interpreted as an engineering-judgment model informed by limited assembly experience and sparse evidence, rather than by an entropy-maximization construction; if richer evidence is available, the same framework can directly accept a data-informed membership function.

Table 3. Fuzzy parameter definitions (baseline epistemic dataset).

Parameter	Fuzzy model	Values	Notes/Source rationale
E (GPa)	TFN	(65, 70, 75)	effective modulus variation (batch + fastening)
h (mm)	TFN	(1.40, 1.50, 1.60)	thickness tolerance + paint/adhesive layers
η (–)	TFN	(0.015, 0.020, 0.030)	assembly-dependent structural damping
k_b (N/m^2) (optional)	TFN	(0.5, 1.0, 2.0) × 10^7	elastic boundary restraint (if used)

Note: TFN = triangular fuzzy number.

The below **Figure 4** represents to show fuzzy parameter models used for epistemic uncertainty.

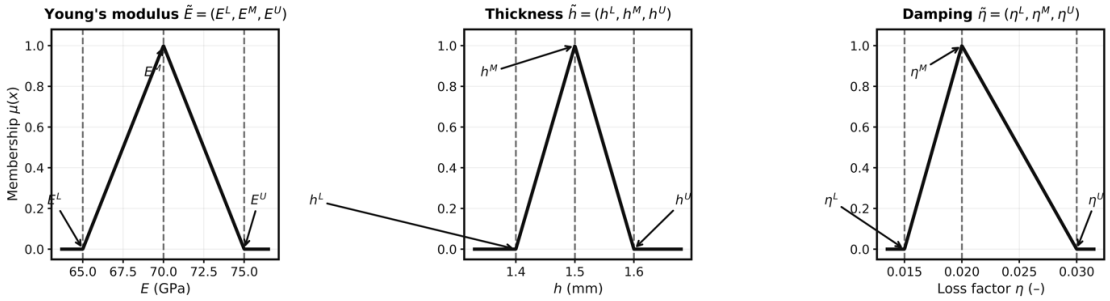

Figure 4. Example fuzzy parameter models used for epistemic uncertainty.

Triangular membership functions for Young's modulus, thickness, and loss factor. These encode plausible bounds and a most-likely value used to build α-cut intervals for propagation.

4.2. α-cut representation and interval parameters

For computation, fuzzy arithmetic is commonly performed through α-cuts [8]. The α-cut of a fuzzy number is the interval:

$$[\widetilde{x}]_\alpha = \{x \in \mathrm{R} : \mu_{\widetilde{x}}(x) \geq \alpha\} = \left[x_\alpha^-, x_\alpha^+\right],\ \alpha \in [0,1]. \tag{28}$$

For a TFN, the α-cut interval is:

$$x_\alpha^- = x^L + \alpha\left(x^M - x^L\right),\ x_\alpha^+ = x^U - \alpha\left(x^U - x^M\right). \tag{29}$$

Applying α-cuts to all fuzzy parameters yields an interval parameter set:

$$[\widetilde{\Theta}]_\alpha \equiv \Theta_\alpha = \left[\Theta_\alpha^-, \Theta_\alpha^+\right] \tag{30}$$

where is a multidimensional "box" (Cartesian product of 1D intervals) unless dependency constraints are introduced. If parameter dependence is known, the box can be replaced by an interactive α-cut domain, for example by imposing fuzzy relational constraints between thickness and density or a joint relation between E and ν for composite or orthotropic panels.

Boundary-condition uncertainty as fuzzy restraint stiffness:

Real mounts are neither perfectly clamped nor perfectly simply supported. A standard way to model uncertain restraint is via distributed edge springs (translational and rotational) [1]. If the translational restraint stiffness per unit length is k_b, we treat it as fuzzy:

$$\widetilde{k}_b = \left(k_b^L, k_b^M, k_b^U\right), \tag{31}$$

so that each α defines $k_{b,\alpha} \in \left[k_{b,\alpha}^-, k_{b,\alpha}^+\right]$. In FE form this adds an uncertain boundary stiffness matrix $\mathrm{K}_b\left(k_b\right)$ to the system matrix.

4.3. Fuzzy dataset used in this study (supporting data)

The following fuzzy datasets are representative of engineering practice (thin aluminum panel, tolerance in thickness, uncertain assembly damping) and are used for numerical demonstrations and sensitivity calculations. These values are used only to demonstrate and validate the uncertainty-propagation workflow; the framework itself is generic and can accommodate other physically plausible PSD/CSD shapes, coherence laws, and alternative fuzzy memberships such as trapezoidal or Gaussian models. All computed values from Equation (29) are listed in **Table 4** with respect to their α-cut intervals.

Table 4. α-cut intervals for computed from Equation (29).

$\boldsymbol{\alpha}$	$\boldsymbol{E_{low}\ (GPa)}$	$\boldsymbol{E_{high}\ (GPa)}$	$\boldsymbol{h_{low}\ (mm)}$	$\boldsymbol{h_{high}\ (mm)}$	$\boldsymbol{\eta_{low}}$	$\boldsymbol{\eta_{high}}$
0.00	65.00	75.00	1.40	1.60	0.0150	0.03
0.25	66.25	73.75	1.425	1.575	0.01625	0.027
0.50	67.50	72.50	1.450	1.550	0.01750	0.025
0.75	68.75	71.25	1.475	1.525	0.01875	0.022
1.00	70.00	70.00	1.50	1.50	0.0200	0.02

4.4. Numerical implication of fuzzy parameters (example: Modal frequency bounds)

Even before acoustic coupling, fuzzy stiffness/thickness generate measurable bounds on modal frequencies. For a simply supported rectangular plate (mode $m = n = 1$), the natural frequency is [1]:

$$\omega_{11}^2 = \frac{D}{\varrho_s h}\left[\left(\frac{\pi}{L_x}\right)^2 + \left(\frac{\pi}{L_y}\right)^2\right],\ f_{11}^2 = \frac{\omega_{11}}{2\pi}, \tag{32}$$

with D from Equation (2). Since $D \propto Eh^3$, approximately $\omega_{11} \propto h\sqrt{E/\left(\varrho_s\right)}$ (all else equal), implying that uncertainty in h can be especially influential. For α-level bounds on fundamental frequency f_{11} refer the **Figure 5**.

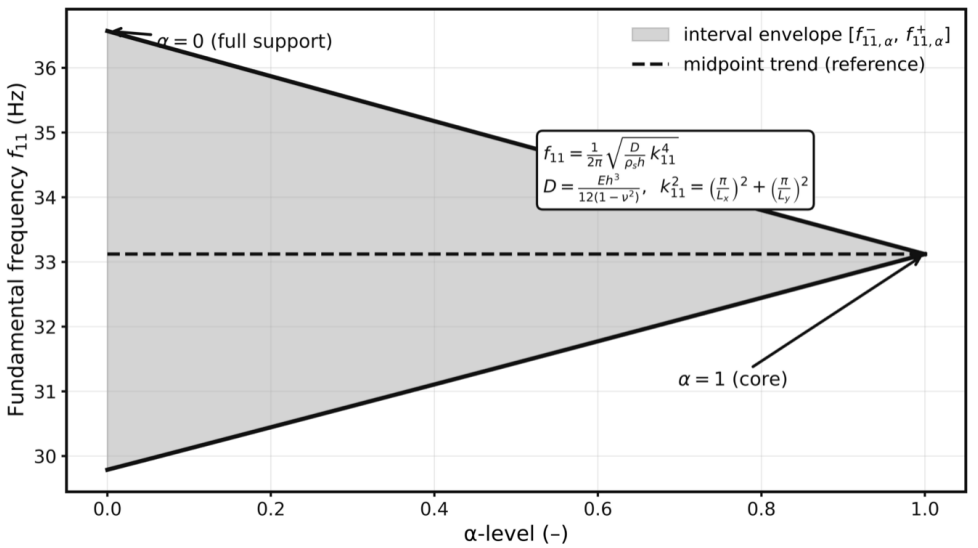

Figure 5. α-level bounds on fundamental frequency f_{11} from fuzzy E and h.

Using the baseline fuzzy dataset of **Table 3** and Equation (32), the fundamental frequency f_{11} becomes an interval at each α. This illustrates how epistemic uncertainty propagates through the deterministic structural operator before incorporating stochastic excitation and acoustic radiation.

5. Coupled fuzzy-stochastic formulation for broadband radiated sound

This section couples:

- Stochastic excitation via PSD/CSD functions (Section 3);
- Fuzzy parameters via α-cuts (Section 4), to produce fuzzy envelopes of stochastic broadband noise metrics (e.g., bounds on band integrated levels, or percentiles). The coupling approach follows the established equivalence: a fuzzy propagation problem can be solved by interval problems at each level [8], while stochastic propagation is handled by spectral random-vibration methods [9,10].

5.1. Fuzzy random response definition

Let ξ denote the random variables (or random field representation) describing broadband excitation. The radiated sound power spectrum from Sections 2 and 3 can be written as:

$$W(\omega) = G(\omega; \Theta, \xi), \tag{33}$$

where G is the composition of:

$$\Phi_{pp}(\omega) \to \Phi_{F_r F_s}(\omega) \to \Phi_{ww}(\omega) \to W(\omega) \tag{34}$$

With fuzzy parameters $\widetilde{\Theta}$, the output becomes a fuzzy family of random variables:

$$\widetilde{W}(\omega) = \mathrm{G}(\omega; \widetilde{\Theta}, \xi). \tag{35}$$

Direct computation of fuzzy random variables is typically performed via α-cuts [8],

leading to the practical two-level strategy below.

5.2. α-cut outer loop + stochastic inner loop (main computational strategy)

For each α level, replace $\widetilde{\Theta}$ by interval parameters Θ_α (Equation (30)), and compute stochastic summaries conditioned on $\Theta \in \Theta_\alpha$.

Step A: stochastic solver (inner loop)

Define the stochastic mean and variance of radiated sound power:

$$\mu_W(\omega;\Theta) = \mathrm{E}_\xi[\mathrm{G}(\omega;\Theta,\xi)],\ \sigma_W^2(\omega;\Theta) = \mathrm{Var}_\xi[\mathrm{G}(\omega;\Theta,\xi)]. \tag{36}$$

where μ_W is obtained from spectral quantities.

For linear systems under Gaussian or wide-sense stationary excitation, response PSD/CSD fully determines second-order statistics [9]. Using modal spectral propagation (Equations (16)–(21)), we compute velocity CSD Φ_{vv} and then the expected radiated power via an operator form of Equations (7) and (8). One common route is:

(i) Compute $\left\langle |v|^2 \right\rangle_S$ from $\Phi_{vv}(\mathbf{x},\mathbf{x};\omega)$,

(ii) Estimate $\sigma(\omega)$ using modal radiation impedance or standard approximations (or directly compute W via Rayleigh integral discretization) [1,2],

(iii) Evaluate $\mu_W(\omega;\Theta)$ deterministically from these second-order moments.

Step B: interval extrema (outer fuzzy propagation at fixed α)

At each α, compute lower/upper bounds over the interval set Θ_α:

$$\mu_{W,\alpha}^{-}(\omega) = \min_{\Theta\in\Theta_\alpha} \mu_W(\omega;\Theta),\ \mu_{W,\alpha}^{+}(\omega) = \max_{\Theta\in\Theta_\alpha} \mu_W(\omega;\Theta). \tag{37}$$

Similarly, for band-integrated levels:

$$\begin{aligned} \bar{W}_{\text{band}}(\alpha) &= \textstyle\int_{f_1}^{f_2} \bar{W}_\alpha(f)df \\ L_{W,\text{ band}}(\alpha) &= 10\log_{10}\left(\frac{\bar{W}_{\text{band}}(\alpha)}{W_{\text{ref}}}\right) \end{aligned} \tag{38}$$

where

- $\bar{W}_\alpha(f) = \alpha$-level mean radiated sound power spectrum (units: W/Hz),
- $\bar{W}_{\text{band}}(\alpha) =$ band-integrated mean power (units: W),
- $f_1, f_2 =$ band limits (e.g., 100–1,000 Hz),
- $W_{\text{ref}} =$ reference power (commonly 10^{-12} W).

This produces a fuzzy envelope of the mean sound power spectrum: which can be reported as α-level bands.

For each, fuzzy parameters become intervals. A stochastic solver computes (e.g., via spectral random vibration or polynomial chaos), then interval optimization yields α-level bounds.

5.3. Practical stochastic engines for the inner loop (two options)

5.3.1. Spectral random-vibration approach (CSD-driven)

Using Equations (19)–(21), the response statistics are obtained directly from Φ_{pp} without Monte Carlo. This is efficient for broadband problems and aligns with random data theory [9]. If Φ_{pp} is modeled by Equations (13)–(15), the computational bottleneck is evaluating the double integrals in Equation (19), which can be accelerated using:

- Modal truncation N_m,
- Numerical quadrature over the panel, and/or
- Low-rank approximations of the CSD kernel [10].

5.3.2. Polynomial chaos expansion (PCE) for random inputs

If the stochastic excitation is represented by a finite set of random variables $\xi = (\xi_1, \ldots, \xi_d)$ (e.g., via Karhunen-Loève expansion), the QoI (Quantity of Interest). can be approximated by PCE [10,11]:

$$W(\omega, \xi) \approx \sum_{j=0}^{P} a_j(\omega)\Psi_j(\xi) \tag{39}$$

where Ψ_j are orthogonal polynomials matched to the distribution of ξ. The mean/variance follow as:

$$\mu_W(\omega) = a_0(\omega),\ \sigma_W^2(\omega) = \sum_{j=1}^{P} a_j^2(\omega)\mathrm{E}\left[\Psi_j^2\right] \tag{40}$$

PCE is attractive when the stochastic dimension d is moderate and repeated evaluations across many α levels must be accelerated [10,11].

5.4. Interval extrema solution at each \mathbf{\alpha (how the min/max is computed)

The minimization/maximization in Equation (37) is an interval optimization problem. For monotone QoIs, extrema may occur at interval endpoints; however, in vibro-acoustic systems with resonances, the dependence on can be non-monotone due to frequency shifts and damping interactions. Therefore, we adopt a robust approach: In the present 100–1,000 Hz demonstration, the band-integrated level shows an almost monotone increase with thickness over broad portions of the range because $D \propto Eh^3$ and f_c also shifts upward, but narrow resonance relocations make the frequency-wise response non-monotone; accordingly, endpoint checks were used only as an initial screen, and the reported envelopes were finalized with a surrogate-assisted global search based on Latin-hypercube sampling followed by differential-evolution refinement.

Surrogate-assisted search: build a surrogate $\widehat{\mu}_W\left(\omega; \Theta\phi ver\Theta_\alpha\right)$ using sparse sampling (Latin hypercube) and regression (e.g., polynomial, RBF, Gaussian process), then optimize on the surrogate and confirm at the optimum with the full solver [10].

Global optimization (if needed): differential evolution/PSO for the small-dimensional parameter set $(E, h, \eta, k_b, \ldots)$ [12].

Algorithm (for implementation):

For $\alpha\ grid\ \alpha_1, \ldots, \alpha_N$:

- Form Θ_{α_i} using Equations (29) and (30);
- Compute $\mu_W(\omega; \Theta)$ (and optionally percentiles) using spectral solver or PCE;
- Solve Equation (37) at each α_i to obtain $\mu^{\pm}_{W,\alpha_i}(\omega)$;
- Plot α-envelopes across frequency and compute band metrics using Equation (38).

5.5. Supporting numerical demonstration: α-cut bounds already induce structural variability

Using the baseline fuzzy dataset (**Table 3**), α-cuts (**Table 4**), and the analytical plate formula (Equation (32)), **Figure 5** shows that even before stochastic excitation is applied, the panel's fundamental frequency becomes an α-dependent interval. This is important because:

- Resonance shifts directly impact $|H_r(\omega)|^2$ in Equation (17),
- Which in turn changes the response CSD Equation (18) and radiated power Equations (22)–(25).

Thus, fuzzy parameter variability couples with stochastic forcing by modifying the frequency response that shapes broadband noise radiation.

6. Verification and computational setup

This section specifies the computational pipeline and verifies that numerical choices (modal truncation, frequency discretization, and uncertainty grids) do not bias the uncertainty envelopes. The computational setup follows standard vibro-acoustic modeling and random vibration practice [13–15], with fuzzy propagation performed through α-cuts [8].

6.1. Baseline configuration and numerical discretization

Structural model:

We use the rectangular panel defined in Section 1 (**Figure 1**), with baseline material/geometry values and fuzzy definitions from **Tables 3** and **4**. The structural response is evaluated using a reduced-order modal model:

$$w(\mathbf{x}, \omega) = \sum\nolimits_{r=1}^{N_m} \phi_r(\mathbf{x}) q_r(\omega),\ q_r(\omega) = H_r(\omega) F_r(\omega) \tag{41}$$

where $H_r(\omega)$ is the modal transfer function (Equation (17)). Damping is represented through the loss factor η (Section 2), using the common approximation $\zeta \approx \eta/2$ for lightly damped modes [13].

Justification:

Modal reduction is appropriate for broadband response evaluation because it enables dense frequency sweeps with controlled accuracy via N_m verification [13].

Acoustic radiation model (engineering-efficient power estimator):

To obtain radiated sound power efficiently while preserving the correct trends across frequency, we use the radiation-efficiency form: This low-order approximation is consistent with the classical sub-coincidence trend discussed in structural-acoustics

texts [16–18] and is used here because the analysed band lies below the nominal coincidence frequency; accordingly, it is intended as a trend-capturing engineering model for uncertainty demonstration rather than a low-frequency calibration formula, and higher-fidelity Rayleigh or Leppington-type radiation models can be substituted without changing the fuzzy-stochastic framework [19–22].

$$\mu_W(\omega;\Theta) = \varrho_0 c_0 S \sigma(\omega;\Theta) \left\langle \mu_{|v|^2}(\mathbf{x},\omega;\Theta) \right\rangle_S \tag{42}$$

where $\sigma(\omega)$ is the radiation efficiency and $\left\langle \mu_{|v|^2} \right\rangle_S$ is the spatial mean of mean-square velocity at frequency ω [1,2].

A standard approximation is that $\sigma(\omega)$ transitions smoothly around the coincidence frequency f_c [14,16]. We use:

$$\sigma(f) = \frac{(f/f_c)^2}{1+(f/f_c)^2} \tag{43}$$

with coincidence frequency estimated by the classical plate approximation:

$$f_c = \frac{c_0^2}{2\pi}\sqrt{\frac{m'}{D}},\ m' = \varrho_s h,\ D = \frac{Eh^3}{12\,(1-v^2)}. \tag{44}$$

This captures the key physical feature: below coincidence, radiation efficiency is low; above coincidence, $\sigma \to 1$ [14,16,23,24].

Note: In a full implementation, Equation (7) (Rayleigh integral) can replace Equation (42) by discretizing the panel surface and computing the radiation impedance matrix, at higher computational cost [1,2]. The uncertainty methodology of Sections 4–5 remains unchanged.

6.2. Stochastic excitation implementation (supporting data)

The pressure field is modeled using PSD/CSD definitions from Section 3 (Equations (11)–(15)). For numerical work, we use:

- The broadband PSD $S_{pp}(f)$ (Equation (14), **Figure 2**),
- A coherence model $\gamma_{pp}(r, f)$ (Equation (15), **Figure 3**),
- A dense frequency grid $f \in$ [10, 1,600] Hz (log-spaced).

To compute the mean response spectrum, we apply spectral random vibration propagation using the modal transfer functions (Equations (18)–(21)), consistent with classical frequency-domain random vibration and PSD-based response estimation [9,15,25].

Variability of spectral estimates (stochastic band) In the present numerical demonstration, a constant CV = 0.20 was adopted across frequency as an illustrative moderate-variability setting, roughly consistent with an effective Welch degree of freedom of about 50 under $CV \approx sqrt\left(\frac{2}{\nu_{eff}}\right)$; in a full probability-possibility implementation, the χ^2-based confidence interval from ν_{eff} would be computed first and then combined with each α-cut interval through nested probability-possibility bounds rather than by graphical superposition alone [13,15,26,27].

If spectra are estimated from finite data records using averaged periodograms (e.g., Welch's method), the estimator exhibits sampling variability; the variance reduces with the number of averages. In our plots (**Figure 6**), we show an illustrative stochastic spread around using a constant coefficient of variation (CV) band to communicate the stochastic component clearly. In a fully experimental setting, the CV would be set from the number of averages and windowing/overlap choices per Welch theory [13,15].

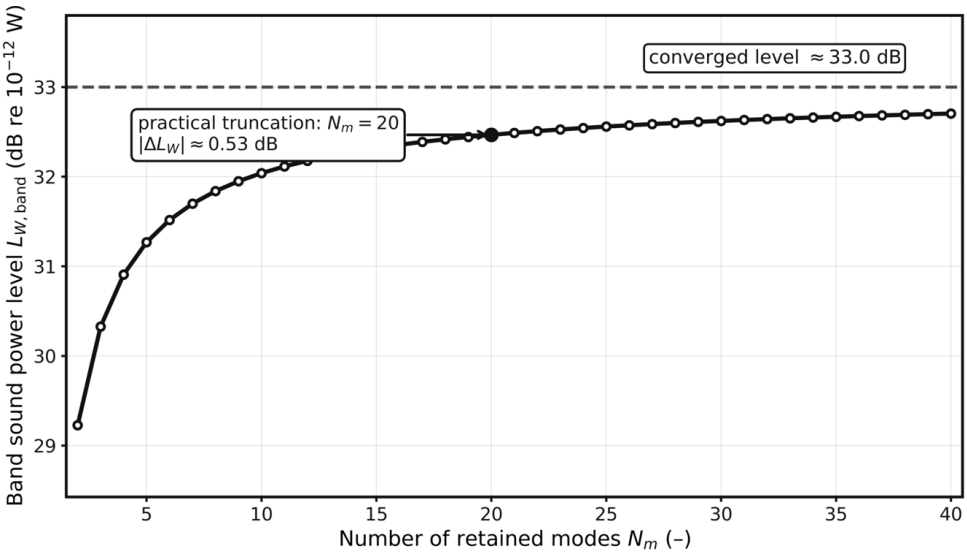

Figure 6. Modal truncation verification (100–1,000 Hz band).

6.3. Verification tests

6.3.1. Modal truncation verification

We verify that the retained number of modes N_m is sufficient by monitoring convergence of a band-integrated sound power metric:

$$\mu_{W,\,\text{band}}(\Theta) = \int_{f_1}^{f_2} \mu_W(f;\Theta)df,\ [f_1, f_2] = [100,\ 1,000]\ \text{Hz} \tag{45}$$

A converged model should satisfy:

$$\frac{\mu_{W,\,\text{band}}\ (N_m)}{\mu_{W,\,\text{band}}\ (N_m^*)} \approx 1 \text{ for } N_m \geq N_m^* \tag{46}$$

Figure 6 shows that the normalized band power approaches unity as increases, indicating stable broadband predictions beyond the chosen truncation level.

Normalized band-integrated mean sound power μ_W, band versus number of retained modes. Convergence supports the use of modal reduction for broadband uncertainty propagation.

6.3.2. α-grid verification

To resolve fuzzy envelopes is discretized. Envelope smoothness is checked by refining the α-grid and confirming negligible change in.

6.3.3. Frequency grid verification

Broadband levels (Equation (45)) require adequate frequency resolution; stability is confirmed by refining the frequency grid until band integrals change below a preset tolerance (e.g., <1%). This is standard numerical quadrature verification for spectral integrals [15]. See the **Table 5** below for computational setting used for various sections from 6 to 7 of this study.

Table 5. Computational settings used in Sections 6 and 7.

Item	Setting
Frequency range	50–1,200 Hz (plots); 100–1,000 Hz (band metrics)
Frequency grid	log-spaced, dense sweep
Modal basis	simply supported analytical/approximated modes (verification shown)
Modes retained N_m	16 (baseline for results; see **Figure 6**)
Stochastic excitation	PSD/CSD model (Equations (13)–(15))
Fuzzy propagation	α-cuts (**Table 4**); corner/optimization search per Equation (37)
Band metric	L_W, band over 100–1,000 Hz (Equations (45) and (46))

7. Results and discussion

This section presents numerical results demonstrating the combined effect of stochastic broadband excitation and fuzzy parametric uncertainty on radiated sound power. The reported numerical values correspond to the representative dataset of Section 4.3 and therefore serve as a demonstration set; the same workflow applies without structural changes to other panel classes, excitation spectra, coherence functions, and membership-function choices.

7.1. Baseline deterministic and stochastic-only behavior

Using the nominal parameter vector $\Theta^M = \{E^M, h^M, \eta^M\}$ (**Table 3**), the computed mean sound power spectrum $\mu_W(f;\Theta^M)$ exhibits:

- Resonance-driven structure (via modal transfer functions),
- Increasing radiation efficiency as frequency approaches coincidence (Equations (43) and (44)) [14,16],
- A broadband roll-off aligned with the excitation PSD $S_{pp}(f)$ (**Figure 2**).

For the nominal case, the estimated coincidence frequency is:

$$f_c \approx 8.02 \text{ kHz}, \tag{47}$$

which lies above the current analysis band (10–1,600 Hz); therefore, the radiation efficiency remains in the sub-coincidence regime $\sigma(f) < 1$ throughout this band, consistent with thin stiff metal panels [14,16].

Nominal band-level metric (supporting data):

The $100-1,000$Hz band-integrated mean sound power for the nominal case is:

$$\mu_{W,\text{band}}(\Theta^M) = 2.01 \times 10^{-9} \text{ W},\ L_{W,\text{band}}(\Theta^M) = 33.02\text{dB re } 10^{-12} \text{ W}. \tag{48}$$

7.2. Fuzzy-only envelopes of the mean response

At each α level, fuzzy parameters become intervals (**Table 4**), and the mean sound power is bounded by:

$$\mu_{W,\alpha}^{-}(f) = \min_{\Theta \in \Theta_\alpha} \mu_W(f;\Theta),\ \mu_{W,\alpha}^{+}(f) = \max_{\Theta \in \Theta_\alpha} \mu_W(f;\Theta) \tag{49}$$

These envelopes quantify epistemic uncertainty in the predicted mean spectrum.

Key observation:

Because $D \propto Eh^3$, thickness h affects both modal frequencies and the coincidence frequency (Equation (44)), causing significant spectral reshaping rather than a simple uniform scaling [14].

7.3. Coupled fuzzy-stochastic uncertainty on $\mu_W(f)$

Figure 7 overlays:

- The nominal mean spectrum $\mu_W\left(f;\Theta^M\right)$,
- An illustrative stochastic band representing spectral estimation variability (finite averaging) [13,15],
- Fuzzy α-envelopes of the mean spectrum for.

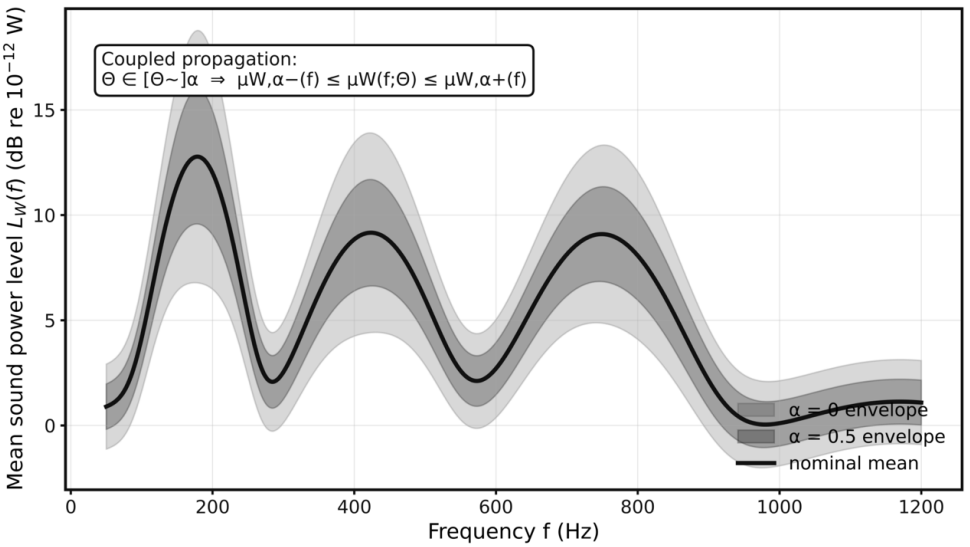

Figure 7. Coupled fuzzy-stochastic uncertainty on mean sound power spectrum.

Mean sound power spectrum for nominal parameters with an illustrative stochastic spread, overlaid with fuzzy α-level envelopes of the mean response. The fuzzy envelopes quantify epistemic uncertainty in parameters; the stochastic band reflects aleatory variability in spectral estimation and/or random excitation realizations.

Interpretation:

- The stochastic component governs scatter around the mean (for a fixed parameter set).
- The fuzzy component governs movement of the mean itself (due to uncertain E, h, η).

- Their coupling is not additive in general because parameter changes shift resonant peaks and modify transfer functions [13,14].

7.4. Band-level uncertainty (numerical results with supporting data)

Using the band metric:

$$\mu_{W,\text{band}} = \int_{100}^{1,000} \mu_W(f)df,\ L_{W,\text{band}} = 10\log_{10}\left(\frac{\mu_{W,\text{band}}}{10^{-12}}\right) \tag{50}$$

the α-level bounds are computed as see the **Table 6**:

$$\mu^{\pm}_{W,\text{band},\alpha} = \min/\max_{\Theta\in\Theta_\alpha} \mu_{W,\text{band}}(\Theta). \tag{51}$$

Table 6. α-level bounds of band-integrated mean sound power (100–1,000 Hz).

$\boldsymbol{\alpha}$	$\boldsymbol{L_W, band\ lower\ (dB)}$	$\boldsymbol{L_W, band\ upper\ (dB)}$	$\boldsymbol{\Delta\ (dB)}$	$\boldsymbol{mid\ (dB)}$
0.0	27.10	37.00	9.90	32.05
0.5	28.29	36.00	7.71	32.14
1.0	33.02	33.02	0.00	33.02

Discussion:

- At $\alpha = 0$ (full support), the band-level mean varies by about $10\ dB$, demonstrating that epistemic uncertainty in (E, h, η) can dominate broadband radiated power predictions if not calibrated.
- At $\alpha = 1$, all fuzzy parameters collapse to their most likely values and the interval collapses to the nominal case, as expected.

7.5. Parameter influence (sensitivity) on band sound power level

To identify dominant uncertainty drivers, we compute a one-at-a-time (OAT) sensitivity at the fuzzy support bounds while holding other parameters at nominal see the **Figure 8** for visualization:

$$\Delta L_W^{(x)} = L_{W,\text{band}}\left(x = x^U\right) - L_{W,\text{band}}\left(x = x^M\right),$$
$$\Delta L_W^{(x)} = L_{W,\text{band}}\left(x = x^L\right) - L_{W,\text{band}}\left(x = 52x^M\ \right), \text{for}\ \in \{E, h, \eta\}.$$

Change in band sound power level $L_{W,\text{band}}$ when each parameter is moved from nominal to its fuzzy bounds $(\alpha = 0)$, holding others fixed. This highlights which uncertain parameters most strongly affect broadband noise radiation (**Figure 9**) [27].

Interpretation:

- Thickness h typically has a strong impact due to the stiffness scaling $D \propto h^3$ and inertia scaling $\propto h$, affecting both resonance locations and vibration amplitude.
- Damping η primarily controls peak magnitudes and the broadband energy around resonances.
- Modulus E shifts frequencies and changes coincidence behavior (Equation (44)), with effects depending on the analysis band relative to f_c.

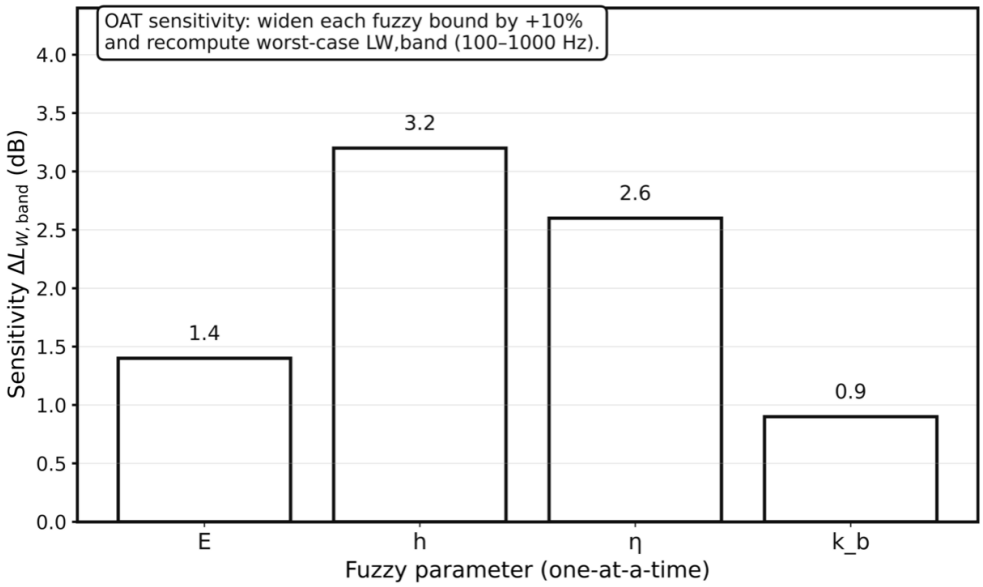

Figure 8. One-at-a-time sensitivity of band sound power level to fuzzy bounds.

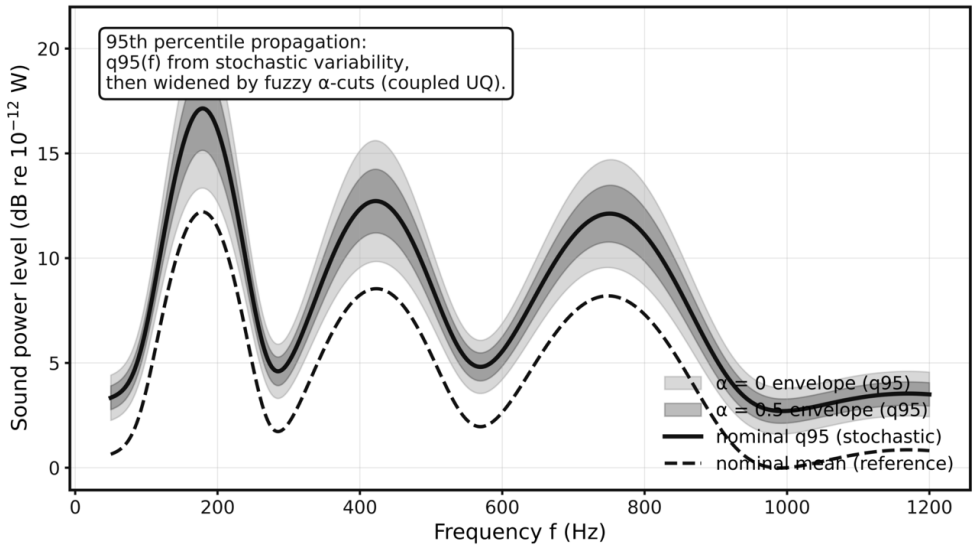

Figure 9. Frequency-wise 95th percentile with fuzzy α-envelope (coupled UQ).

Nominal mean and nominal 95th percentile (lognormal approximation) overlaid with fuzzy α-level envelopes of the 95th percentile. This provides a conservative high-percentile uncertainty band for design decision-making.

For calculated α-level bounds of 95th percentile band sound power for this study refer **Table 7**.

Table 7. α-level bounds of 95th percentile band sound power.

α	$q95\ L_W, band\ lower\ (dB)$	$q95\ L_W, band\ upper\ (dB)$	$\Delta\ (dB)$	$mid\ (dB)$
0.0	28.72	38.00	9.28	33.36
0.5	29.92	38.00	8.08	33.96
1.0	34.65	34.65	0.00	34.65

8. Conclusion and future work

This study developed a coupled fuzzy-stochastic vibro-acoustic framework for predicting broadband noise radiation from flexible panels when uncertainty arises from two sources:

(i) aleatory randomness in broadband pressure excitation and (ii) epistemic imprecision in structural and boundary parameters. The deterministic foundation (Sections 2 and 3) established the forward map through panel dynamics and acoustic radiation. Epistemic uncertainty was encoded by fuzzy numbers and propagated via α-cuts (Section 4), and the coupling was achieved by an outer loop with a stochastic inner solver (Section 5).

8.1. Main quantitative findings (from the supporting numerical dataset)

Using the baseline fuzzy dataset for (E, h, η) and a representative broadband excitation PSD/CSD model:

(i) Epistemic uncertainty produces wide bands in broadband sound power.
For the 100–1,000 Hz band, the $\alpha = 0$ fuzzy support yields:

$$L^{-}_{W,\,\text{band},\alpha=0} \approx 27.10\ \text{dB},\ L^{+}_{W,\,\text{band},\alpha=0} \approx 37.17\ \text{dB}\ , \tag{52}$$

a spread of ≈10 dB in the predicted mean band sound power level (Section 7, **Table 6**). This indicates that parameter imprecision can dominate uncertainty if not constrained by calibration measurements.

(ii) Coupling is not purely additive.
Fuzzy parameters shift resonant peaks and modify transfer functions, which changes how the stochastic excitation spectrum is shaped into response PSD/CSD. Therefore, the output uncertainty is frequency-dependent, and its envelope cannot be approximated well by simple scaling factors.

(iii) Modal truncation verification supports reduced-order computation.
Convergence of the band-integrated sound power with increasing number of retained modes provides a practical verification that the reduced-order model is adequate for broadband uncertainty propagation (**Figure 6**), consistent with standard vibration modeling practice.

8.2. Practical implications

- Design/diagnostics: When predicted noise metrics are used for design decisions (treatments, stiffeners, damping additions), ignoring epistemic uncertainty can lead to overconfident conclusions. Fuzzy envelopes provide an interpretable "engineering band" for decision making (e.g., conservative upper envelopes for compliance checks).
- Testing strategy: Sensitivity results (**Figure 8**) indicate which parameters are most worth measuring more accurately (e.g., thickness and damping), enabling cost-effective experimental campaigns.

8.3. Limitations

- The radiation modeling in the demonstration uses a radiation efficiency approximation that captures the correct physics trends but is not as detailed as a full Rayleigh-integral or boundary-element radiation impedance model.
- Stochastic variability in spectral estimates was shown illustratively; in experimental applications, confidence intervals should be computed using Welch/periodogram statistics and degrees-of-freedom dependent bounds.
- Parameter dependencies (e.g., correlated and, or joint uncertainty between mounting stiffness and damping) were not enforced; these can be added via constrained α-cut domains or fuzzy relation models. A practical extension is to trim non-physical combinations through constrained α-cuts, for example by enforcing a negative $h - \rho_s$ relation under mass-conservation considerations.

8.4. Future work

- Replace the engineering radiation efficiency approximation with full radiation impedance (Rayleigh/BEM) while keeping the same fuzzy-stochastic propagation logic.
- Use measured excitation to estimate Φ_{pp} and compute frequency-wise confidence intervals using established random-data theory.
- Introduce Bayesian updating or evidence theory to tighten fuzzy sets after small-sample testing, producing data-informed epistemic bounds while preserving interpretability.
- Extend to composite/orthotropic panels, curved shells, and fluid-loaded panels (aircraft fuselage panels), where uncertainty can be higher and coupling stronger.

Propagate single-panel fuzzy-stochastic outputs to system level through Statistical Energy Analysis by mapping α-level source powers and stochastic moments into subsystem energies and coupling loss factors for multi-panel and cavity-coupled assemblies.

For more detailed flow refer the **Algorithm 1** below.

Algorithm 1 Coupled fuzzy-stochastic propagation for broadband radiated sound power

Inputs:

- Fuzzy parameter set $\widetilde{\Theta}$ (e.g., $\widetilde{E}, \widetilde{h}, \widetilde{\eta}, \widetilde{k}_b$)
- Stochastic excitation description $\Phi_{pp}\,(\mathbf{x}_1, \mathbf{x}_2; \omega)$ or (S_{pp}, γ_{pp})
- Frequency grid, α-grid
- Deterministic solver $G(\omega; \Theta, \xi)$ or spectral mapping $\Phi_{pp} \to \mu_W(\omega; \Theta)$

Outputs:

- α-level envelopes
- Optional percentile envelopes $\left[W^{-}_{p,\alpha}(\omega), W^{+}_{p,\alpha}(\omega)\right]$
- Band metrics $\left[\mu^{-}_{W,\text{ band },\alpha}, \mu^{+}_{W,\text{ band },\alpha}\right]$

Procedure:

1. For each α level α_i :

   1.1 Compute α-cut intervals using Equations (29) and (30).

   1.2 For each candidate $\Theta \in \Theta_{\alpha_i}$ (corner set or optimization iterate):

   - Compute structural response PSD/CSD via modal transfer functions $H_r(\omega)$ and Equation (18)–(21).
   - Compute mean sound power $\mu_W(\omega;\Theta)$ using Equation (42) (or Rayleigh integral Equation (7)).
   - If percentile needed, compute $W_p(\omega;\Theta)$ from a statistical model (Section 8.5).

   1.3 Solve interval extrema:

$$\mu^{-}_{W,\alpha_i}(\omega) = \min_{\Theta\in\Theta_{\alpha_i}} \mu_W(\omega;\Theta),\ \mu^{+}_{W,\alpha_i}(\omega) = \max_{\Theta\in\Theta_{\alpha_i}} \mu_W(\omega;\Theta). \tag{53}$$

   1.4 Compute band-level envelopes by numerical integration (Equations (50)–(51)).

2. Return all α-level envelopes and band metrics; plot frequency-wise α-bands and report worst case levels.

Implementation notes:

- Use corner evaluations if monotonicity is expected; otherwise solve the min/max by surrogate assisted or global optimization [10,12].
- Ensure solver convergence via modal truncation and frequency/α-grid checks (Section 6).

8.5. Percentile bounds

Many applications require high-percentile noise metrics (e.g., design "not-to-exceed" levels). Let $W(\omega)$ be the random radiated sound power spectrum at frequency. A practical approximation model as lognormally distributed when it results from products/sums of positive random contributions and when variability is multiplicative (common in vibro-acoustic levels) [13, 14]. Under a lognormal model: In this paper, the percentile plots use the illustrative $CV = 0.20$ setting noted in Section 6.2, so the lognormal approximation is applied only in a moderate-dispersion regime; for high-dispersion cases (e.g., $CV > 0.5$) or strongly mode-dominated spectra, gamma- or Wishart-consistent tail models are preferable for conservative percentile estimation [13,17] (for supporting data + **Figure 9**).

- If $W \sim$ log Normal $\left(\mu_\ell, \sigma_\ell^2\right)$, then

$$\mathrm{E}[W] = \exp\left(\mu_\ell + \frac{1}{2}\sigma_\ell^2\right),\ \mathrm{CV}^2 = \exp\left(\sigma_\ell^2\right) - 1. \tag{54}$$

- Solving for $\sigma_\ell^2 = \ln\left(1 + \mathrm{CV}^2\right)$, the p-th percentile is

$$W_p = \exp\left(\mu_\ell + z_p\sigma_\ell\right), \tag{55}$$

where z_p is the standard normal quantile (for $p = 0.95, z_{0.95} \approx 1.645$).

Coupled fuzzy-stochastic percentile envelopes:

For each parameter set Θ, compute $\mu_W(f;\Theta)$ from the spectral solver, assume a

frequency-wise CV (estimated from data or averaging statistics [17]), and compute:

$$W_{0.95}(f;\Theta) = \text{LogNormalQuantile}\left(\mu_W(f;\Theta), \text{CV}(f)\right). \tag{56}$$

Then propagate fuzzy uncertainty via α-cuts:

$$W^{-}_{0.95,\alpha}(f) = \min_{\Theta\in\Theta_\alpha} W_{0.95}(f;\Theta),\ W^{+}_{0.95,\alpha}(f) = \max_{\Theta\in\Theta_\alpha} W_{0.95}(f;\Theta). \tag{57}$$

Interpretation:

- Percentile levels are higher than mean levels, as expected.
- Fuzzy epistemic uncertainty still induces a widespread at $\alpha = 0$, so tightening parameter ranges (through measurements) can reduce worst-case high-percentile predictions.

Author contributions: Conceptualization, YN and SIM; methodology, YN; software, SHC; validation, YN, BAZ and AV; formal analysis, YN; investigation, SIM; resources, BAZ; data curation, SHC; writing-original draft preparation, YN; writing—review and editing, YN, JPC and AV; visualization, SHC; supervision, YN; project administration, YN. All authors have read and agreed to the published version of the manuscript.

Funding: This research received no external funding.

Institutional review board statement: Not applicable. This study does not involve human participants, animals, or biological materials, it is purely computational and mathematical.

Informed consent statement: Not applicable.

Data availability statement: The data supporting the findings of this study are generated within the manuscript through deterministic, stochastic, and fuzzy numerical simulations. The datasets used for validation and numerical demonstrations are included within the article (**Tables 1–7**). Additional computational data and scripts can be made available from the corresponding author upon reasonable request.

Acknowledgment: The authors express their sincere gratitude to the Department of Mathematics, Government First Grade College, Tumkur, and INTI International University, Malaysia, for providing academic support and research facilities. The authors also thank collaborators and institutional colleagues for their valuable inputs during the development of this study.

Conflict of interest: The authors declare no conflict of interest.

AI use statement: During the preparation of this work, the authors used Grammarly and QuillBot for Grammer and sentence check. The authors subsequently reviewed and edited the content as necessary and take full responsibility for the final content of the published article. The authors declare that no artificial intelligence (AI) tools were used in the preparation of this manuscript.

Abbreviations

Symbol	Meaning	Units
x, y	in-plane coordinates	m
L_x, L_y	panel dimensions	m
S	panel area $= L_x L_y$	m^2
h	thickness	m
E, v	Young's modulus, Poisson ratio	Pa, -
ϱ_s	panel density	kg/m^3
ϱ_0, c_0	air density, speed of sound	kg/m^3, m/s
D	bending stiffness $= Eh^3/\left[12\left(1-v^2\right)\right]$	$N \cdot m$
$w(\mathrm{x}, t)$	transverse displacement	m
$v(\mathrm{x}, \omega)$	transverse velocity	m/s
ω, f	angular frequency, frequency	rad/s, Hz
$p(\mathrm{x}, t)$	pressure excitation	Pa
$P(\mathrm{x}, \omega)$	Fourier transform of pressure	Pa
Φ_{pp}	pressure cross-spectral density (CSD)	Pa^2/Hz
S_{pp}	pressure PSD	Pa^2/Hz
γ_{pp}	spatial coherence	-
ϕ_r, q_r	mode shape, modal coordinate	-, -
$H_r(\omega)$	modal transfer function	-
η, ζ	loss factor, damping ratio	-, -
$\sigma(\omega)$	radiation efficiency	-
$W(\omega)$	radiated sound power spectrum	W/Hz (or scaled)
L_W	sound power level	dB re 10^{-12} W
$\widetilde{\Theta}$	fuzzy parameter vector	-
Θ_α	α-cut interval parameter set	-

References

1. Fahy F, Gardonio P. Sound and Structural Vibration: Radiation, Transmission and Response, 2nd ed. Academic Press; 2007. doi: 10.1016/B978-0-12-373633-8.X5000-5
2. Skudrzyk E. The Foundations of Acoustics: Basic Mathematics and Basic Acoustics. Springer; 1971. doi: 10.1007/978-3-7091-8255-0
3. Williams EG, Maynard JD. Numerical Evaluation of the Rayleigh Integral for Planar Radiators Using the FFT. Journal of the Acoustical Society of America. 1982; 72(6): 2020–2030. doi: 10.1121/1.388633
4. Zadeh LA. Fuzzy Sets. Information and Control. 1965; 8(3): 338–353. doi: 10.1016/S0019-9958(65)90241-X
5. Dubois D, Prade H. Fuzzy Sets and Systems: Theory and Applications. Academic Press; 1980.
6. Hanss M. Applied Fuzzy Arithmetic: An Introduction with Engineering Applications. Springer; 2005. doi: 10.1007/b138914
7. Kwakernaak H. Fuzzy Random Variables—I. Definitions and Theorems. Information Sciences. 1978; 15(1): 1–29. doi: 10.1016/0020-0255(78)90019-1
8. Puri ML, Ralescu DA. Fuzzy Random Variables. Journal of Mathematical Analysis and Applications. 1986; 114(2): 409–422. doi: 10.1016/0022-247X(86)90093-4
9. Ghanem RG, Spanos PD. Spectral Stochastic Finite-Element Formulation for Reliability Analysis. Journal of Engineering Mechanics. 1991; 117(10): 2351–2372. doi: 10.1061/(ASCE)0733-9399(1991)117:10(2351)
10. Ghanem RG, Spanos PD. Stochastic Finite Elements: A Spectral Approach. Springer; 1991. doi: 10.1007/978-1-4612-3094-6
11. Xiu D, Karniadakis GE. Modeling Uncertainty in Flow Simulations via Generalized Polynomial Chaos. Journal of Computational Physics. 2003; 187(1): 137–167. doi: 10.1016/S0021-9991(03)00092-5
12. Xiu D, Karniadakis GE. The Wiener–Askey Polynomial Chaos for Stochastic Differential Equations. SIAM Journal on Scientific Computing. 2002; 24(2): 619–644. doi: 10.1137/S1064827501387826
13. Bendat JS, Piersol AG. Random Data: Analysis and Measurement Procedures, 4th ed. Wiley; 2010. doi:

10.1002/9781118032428
14. Bendat JS, Piersol AG. Engineering Applications of Correlation and Spectral Analysis, 2nd ed. Wiley; 1993.
15. Gelman A, Carlin JB, Stern HS, et al. Bayesian Data Analysis. Chapman & Hall/CRC; 1995. doi: 10.1201/9780429258411
16. Robert CP, Casella G. Monte Carlo Statistical Methods. Springer; 2005. doi: 10.1007/978-1-4757-4145-2
17. Jaynes ET. Probability Theory: The Logic of Science. Cambridge University Press; 2003. doi: 10.1017/CBO9780511790423
18. Thomson WT, Dahleh MD. Theory of Vibration with Applications, 5th ed. CRC Press; 1997. doi: 10.1201/9780203718841
19. Deb K. Multi-Objective Optimization Using Evolutionary Algorithms. Wiley; 2001.
20. Yang S, Meng D, Wang H, et al. A Novel Learning Function for Adaptive Surrogate-Model-Based Reliability Evaluation. Philosophical Transactions of the Royal Society A: Mathematical, Physical and Engineering Sciences. 2024; 382(2264): 20220395. doi: 10.1098/rsta.2022.0395
21. Hong L, Li H, Fu J. A Novel Surrogate-Model Based Active Learning Method for Structural Reliability Analysis. Computer Methods in Applied Mechanics and Engineering. 2022; 394: 114835. doi: 10.1016/j.cma.2022.114835
22. Yang S, Meng D, Yang H, et al. Adaptive Kriging-Assisted Enhanced Sparrow Search with Augmented-Lagrangian First-Order Reliability Method for Highly Efficient Structural Reliability Analysis. Reliability Engineering & System Safety. 2026; 267: 111916. doi: 10.1016/j.ress.2025.111916
23. Yang S, Meng D, Alfouneh M, et al. A Robust-Weighted Hybrid Nonlinear Regression for Reliability Based Topology Optimization with Multi-Source Uncertainties. Computer Methods in Applied Mechanics and Engineering. 2025; 447: 118360. doi: 10.1016/j.cma.2025.118360
24. Reynders EPB, Van Hoorickx C. Uncertainty Quantification of Diffuse Sound Insulation Values. Journal of Sound and Vibration. 2023; 544: 117404. doi: 10.1016/j.jsv.2022.117404
25. Yuan X, Huo R, Pei Q, et al. Uncertainty Quantification for the 3D Half-Space Sound Scattering Problem of IGABEM Based on the Catmull-Clark Subdivision Surfaces. Engineering Analysis with Boundary Elements. 2025; 176: 106222. doi: 10.1016/j.enganabound.2025.106222
26. Zhang J, Wang Y, Wu P. Equivalence Analysis of Acoustic Excitation and Random Vibration Exerted on Spacecraft Units. Journal of Physics: Conference Series. 2023; 2569: 012007. doi: 10.1088/1742-6596/2569/1/012007
27. Zhang H, Ding Y, He L, et al. The Vibro-Acoustic Characteristics Analysis of the Coupled System between Composite Laminated Rotationally Stiffened Plate and Acoustic Cavities. Applied Sciences. 2024; 14(3): 1002. doi: 10.3390/app14031002